ACS Photonics

pubs.acs.org/journal/apchd5

Article

Quantum Sensing of Paramagnetic Spins in Liquids with Spin Qubits in Hexagonal Boron Nitride

Xingyu Gao, Sumukh Vaidya, Peng Ju, Saakshi Dikshit, Kunhong Shen, Yong P. Chen, and Tongcang Li*

Cite This: *ACS Photonics* 2023, 10, 2894–2900

Read Online

ACCESS | Metrics & More | Article Recommendations

ABSTRACT: Paramagnetic ions and radicals play essential roles in biology and medicine, but detecting them requires highly sensitive and ambient-operable sensors. Optically addressable spin color centers in 3D semiconductors are useful for detecting paramagnetic spins due to their sensitivity to spin magnetic noise. However, creating high-quality spin defects near the surface of 3D materials is challenging. Here, we show that spin qubits in hexagonal boron nitride (hBN), a layered van der Waals (vdW) material, can efficiently detect paramagnetic spins in liquids at nanoscales. We create shallow spin defects near the hBN surface, which maintain high-contrast optically detected magnetic resonance (ODMR) in liquids. Then, we detect paramagnetic ions in water using spin relaxation measurements, with a sensitivity of about 10^{-18} mol/$\sqrt{\text{Hz}}$ for Gd^{3+} ions. Finally, we show that paramagnetic ions reduce the contrast of spin-dependent fluorescence, enabling efficient detection by continuous wave ODMR. Our results demonstrate the potential of ultrathin hBN quantum sensors for chemical and biological applications.

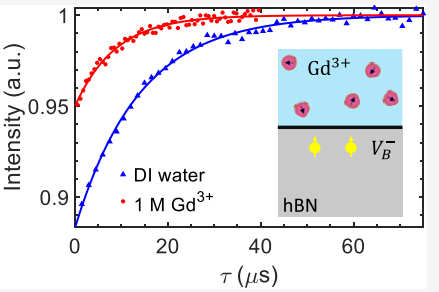

KEYWORDS: *spin defects, hexagonal boron nitride, quantum sensing, paramagnetic ions*

INTRODUCTION

Quantum sensing has emerged as a powerful technique for detecting and measuring a wide range of physical and chemical quantities.[1,2] It has been shown to be highly sensitive and have applications in material science, biology, and medicine.[3−6] Recently, optically active spin defects in hexagonal boron nitride (hBN)[7−10] are emerging as promising platforms for quantum sensing.[11] The 2D nature of hBN allows for spin defects to be embedded in atomically thin layers while maintaining high spin qualities,[12] enabling the sensor to be in close proximity to the target sample, thereby improving sensitivity. Also, a 2D vdW material can be readily integrated into other devices and form multifunctional heterostructures, which opens prospects for in situ quantum sensing.[13] So far, hBN spin defects have been used for sensing multiple physical quantities in solids, including static magnetic fields,[14,15] spin noise in solids,[14,16] temperature,[15,17,18] strain,[19,20] and nuclear spins.[21] However, quantum sensing of paramagnetic ions in liquids with hBN spin defects has not been reported, even though paramagnetic ions play critical roles in chemical, biological, and medical sciences. It is still not clear whether water may degrade the properties of shallow hBN spin defects.[22]

Paramagnetic ions and radicals contain at least one unpaired electron and are involved in various physiological processes including cell signaling[23] and immune response to infection.[24] Some paramagnetic ions can be potentially used as biomarkers for monitoring disease states.[25] For example, gadolinium ions (Gd^{3+}) are widely invoked as relaxation agents and play a major role in magnetic resonance imaging (MRI).[26−29] Iron ions participate in many activities in the human body, including oxygen transport, enzyme function, and mitochondrial energy provision.[30,31] The detection of paramagnetic ions under physiological conditions is highly desired due to their multiple roles in biological and medical sciences.

Previous studies have shown that optically addressable spin color centers in bulk 3D materials, such as nitrogen vacancy (NV) center in diamond, can be used as promising sensors for detecting paramagnetic spins.[32−38] The measurements rely on detecting magnetic noise from fluctuating spins of paramagnetic ions. However, the noise signal Γ decays significantly as the distance d between the sensor and target spins increases, following $\Gamma \propto 1/d^6$ for a single target spin. Therefore, these measurements require the sensor to be in close proximity to the target samples. However, creating high-quality spin color centers near the surface of 3D bulk materials remains challenging due to the inevitable dangling bonds on the surface of bulk 3D materials.

Received: May 9, 2023
Published: July 12, 2023

https://doi.org/10.1021/acsphotonics.3c00621
ACS Photonics 2023, 10, 2894−2900

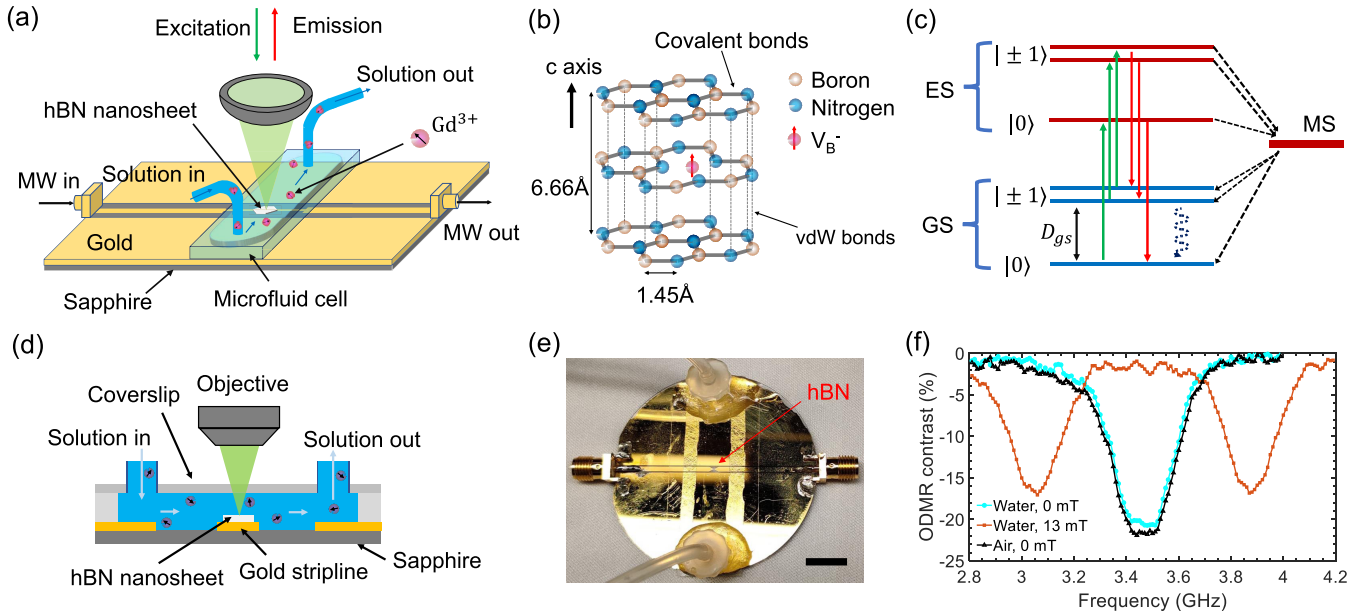

Figure 1. In-solution quantum sensing with shallow spin defects in hBN. (a) Schematic of the experimental setup. An hBN nanosheet with V_B^- spin defects is transferred onto a gold stripline microwave (MW) waveguide on a sapphire substrate. A glass coverslip is placed on top of the waveguide and spaced by double-sided tapes. Two tubes are connected to two sides of the coverslip for delivering and switching solutions. The device is sealed with epoxy. An objective lens focuses a 532 nm green laser to excite V_B^- defect spins and collects the emission from V_B^- defect spins. A microwave is delivered by the waveguide to drive spin defects. (b) Atomic structure of a V_B^- defect. The *c*-axis is perpendicular to the hBN 2D lattice. (c) Simplified energy levels of a V_B^- defect, which include a triplet ($S = 1$) ground state, a triplet ($S = 1$) excited state, and a singlet metastable state. (d) Schematic of the microfluid channel. Gd^{3+} ions in water are slowly pumped into the fluid cell through the tubes. (e) Picture of the microfluid channel on a gold stripline microwave waveguide. The hBN nanosheet is at the center narrow regime of the gold stripline. The scale bar is 1 cm. (f) ODMR spectra of hBN V_B^- spin defects in water without a magnetic field (blue circles), in water with a 13 mT magnetic field (red squares) and in air without a magnetic field (black triangles). The microwave power is 1 W, and the excitation laser power is 3 mW. The experiment is performed at room temperature.

Spin defects in hBN[17,39] provide a promising solution to the challenges of creating high-quality spin color centers near surfaces.[12,40] hBN can be stable at the limit of a monolayer and have no dangling bond on the surface. Spin defects can be readily created close to the hBN surface while sustaining high stability and spin properties without any further surface treatment. Moreover, hBN can be exfoliated into thin flakes and produced in large quantities, which can significantly reduce the cost of production. Here, we report the first quantum sensing of Gd^{3+} paramagnetic ions in liquids using negatively charged boron vacancy (V_B^-) spin defects in hBN in a microfluid structure (Figure 1a). Employing spin relaxometry, we observe a reduction of T_1 relaxation time in the presence of paramagnetic ions. We also present a sensing technique based on the contrast of photoluminescence (PL) emission with and without microwaves. Our results offer new opportunities for the development of highly sensitive and portable sensors for paramagnetic ions with potential applications in medicine, biology, and chemistry.

METHODS

The V_B^- spin defect is a color center in hBN consisting of a missing boron atom at its lattice site in a negatively charged state[7,41−45] (Figure 1b). The symmetry axis of V_B^- defects is always along the c-axis perpendicular to the hBN 2D lattice, making V_B^- well suited for ensemble measurements. The V_B^- has an $S = 1$ triplet ground state with a zero field splitting of $D_{gs} \approx$ 3.47 GHz (Figure 1c). The spin-dependent PL emission, together with spin polarization via laser excitation, enables optically detected magnetic resonance (ODMR) experiments. Our sensors are composed of ensembles of V_B^- defects in hBN nanosheets, created by low-energy helium ions. The average depths (d) of V_B^- defects are 6.4 nm for Sensor 1 (created using a 600 eV He^+ ion beam with a dose density of 10^{15} cm^{-2}) and 4.5 nm for Sensor 2 (created using a 400 eV He^+ ion beam with a dose density of 5×10^{13} cm^{-2}),[46] enabling small sensor-sample separations. The thickness of the hBN nanosheet is typically in the range of 30−50 nm for achieving a strong plasmonic enhancement of the PL intensity on a gold microwave waveguide.[12] The lateral size of the hBN nanosheet is usually larger than 10 μm.

Figure 1a,d illustrates our experimental setup for sensing paramagnetic ions with shallow spin defects in hBN. First, we transfer an hBN nanosheet with V_B^- defects onto a gold microwave transmission line with a width of 35 μm. A coverslip is then placed on top of the microwave waveguide, spaced by double-sided tapes. Two pipes are connected to the two sides of the coverslip for delivering and changing solutions, and the entire device is sealed with epoxy to form a microfluid cell. Figure 1e shows a picture of the prepared device. In the experiment, we use a green laser (532 nm) to excite the V_B^- defects, and collect photon emission with a 750 nm long pass filter. A confocal PL map shows the nearly homogeneous distribution of V_B^- defects over the hBN nanosheet. We first characterize V_B^- spin defects in the transferred hBN nanosheet in air. We then slowly inject deionized (DI) water into the microfluid cell. Continuous wave (CW) ODMR measurements confirm that V_B^- defects maintain high-contrast (about 20%) ODMR signals in the liquid environment (Figure 1f). In the

https://doi.org/10.1021/acsphotonics.3c00621
ACS Photonics 2023, 10, 2894−2900

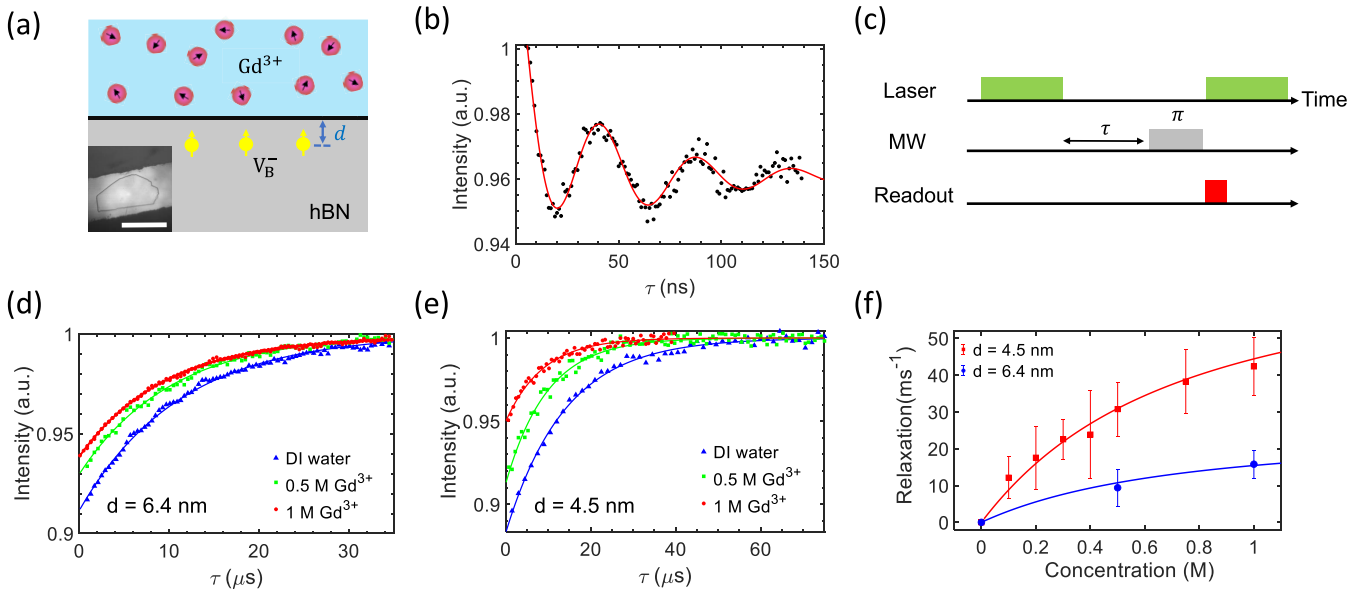

Figure 2. Effects of liquid paramagnetic ions on T_1 of shallow hBN spin defects. (a) Illustration of paramagnetic ions in a liquid that induce spin relaxation in nearby spin qubits. The average depths d of V_B^- defects from the top hBN surface are 6.4 nm for Sensor 1 and 4.5 nm for Sensor 2. Inset: An optical image of an hBN nanosheet on the gold waveguide. The scale bar is 35 μm. (b) Rabi oscillation of V_B^- spin defects measured in water at 13 mT. The Rabi frequency is fitted as f_{Rabi} = 21.6 MHz. (c) Schematic of the pulse sequence for T_1 relaxometry measurements. An initial pumping laser polarizes the V_B^- defect spins to $|m_s = 0\rangle$. After a waiting time of τ, a microwave π pulse followed by another laser pulse is applied to read out the final spin state. (d) Experimental results of T_1 relaxometry in DI water and Gd^{3+} solutions for sensor 1 (d = 6.4 nm). Two different concentrations of Gd^{3+} are used here. The relaxation times are fitted as 11.24 ± 0.17, 10.17 ± 0.50, and 9.54 ± 0.32 μs for DI water (blue triangles), 0.5 M Gd^{3+} solution (green squares), and 1 M Gd^{3+} solution (red circles), respectively. (e) Experimental results of T_1 relaxometry in DI water and Gd^{3+} solutions for sensor 2 (d = 4.5 nm). The relaxation times are fitted as 13.9 ± 0.75, 9.75 ± 0.59, and 8.74 ± 0.51 μs for DI water (blue triangles), 0.5 M Gd^{3+} solution (green squares), and 1 M Gd^{3+} solution (red circles), respectively. (f) Experimental and theoretical results of Gd^{3+}-induced spin relaxation rates as functions of Gd^{3+} concentration for two different average depths.

following discussion, all experiments are performed in liquids, and DI water is used to characterize V_B^- defects as a reference.

RESULTS

We use spin relaxometry to detect surrounding paramagnetic ions by measuring the spin relaxation time (T_1) of shallow V_B^- spin defects (Figure 2a). In a low magnetic field, free diffusing paramagnetic ions exhibit a zero average magnetic field but nonzero root-mean-square (RMS) field due to spin fluctuations. Such stochastic fields can speed up spin relaxation of nearby spin qubits. In our experiment, we first perform coherent control of the V_B^- spins and extract the Rabi frequency for generating a π pulse for T_1 relaxometry measurements. A 1.5 μs green laser pulse is used for spin initialization and readout, and a microwave pulse is used to drive the spin to oscillate between the $|m_s = 0\rangle$ and $|m_s = -1\rangle$ states. As shown in Figure 2b, by varying the microwave pulse duration, we see an oscillation of the PL intensity with a period of around 46.3 ns (f_{Rabi} = 21.6 MHz). Then, the longitudinal relaxation time T_1 is characterized by using the pulse sequence as depicted in Figure 2c. In DI water, the $T_{1,DI}$ of Sensor 1 (d = 6.4 nm) is measured to be 11.24 ± 0.17 μs, which is close to T_1 in air for this hBN nanosheet. They are relatively short due to the high doping density that we used to obtain high PL count rates.[47] In the presence of Gd^{3+} ions (prepared by dissolving $Gd(NO_3)_3$ in water), we observe reduced T_1 relaxation times. The measured spin relaxation times are T_1 = 9.54 ± 0.32 μs for 1 M Gd^{3+} ions and T_1 = 10.17 ± 0.50 μs for 0.5 M Gd^{3+} ions (Figure 2d). Using DI water as the reference, the Gd^{3+}-induced spin relaxation rates can be obtained as $\Gamma_{1,Gd} = 1/T_1 - 1/T_{1,DI}$. They are found to be $\Gamma_{1,Gd}$ = 15.8 ± 3.8 ms^{-1} for 1 M Gd^{3+} ions and $\Gamma_{1,Gd}$ = 9.4 ± 5.0 ms^{-1} for 0.5 M Gd^{3+} ions. To improve the detection of spin noise from Gd^{3+} ions, we create V_B^- defects with an averaged depth of 4.5 nm (Sensor 2) that give a smaller distance between the sensor and Gd^{3+} ions. In this case, we observe a more significant reduction of T_1 relaxation time of V_B^- spins from 13.9 ± 0.75 μs in DI water to 8.74 ± 0.51 μs in a 1 M Gd^{3+} solution (Figure 2e). The measured average values are significantly larger than the uncertainties of our measurements, showing that we have detected paramagnetic ions in water with hBN spin defects.

The paramagnetic-ion-induced spin relaxation rates $\Gamma_{1,Gd}$ depend on the corresponding RMS magnetic field and its spectral density $S_{Gd}(\omega) = \sqrt{2/\pi}\cdot\omega_{Gd}/[(\omega - \omega_L)^2 + \omega_{Gd}^2]$, where ω_L is the Larmor frequency of Gd^{3+} and ω_{Gd} is the composite relaxation rate of Gd^{3+} spins, which is on the order of tens of gigahertz. In a low magnetic field, ω_L is negligible compares to ω_{Gd}, and hence S_{Gd} is dominated by statistical polarization and substantial broadening effects of fluctuations.[32] When the thickness of the Gd^{3+} solution is far larger than the average depth d of V_B^- spins, we can assume that Gd^{3+} ions exist everywhere in the half-infinite space above hBN. Then, the Gd^{3+} induced decay rate $\Gamma_{1,Gd}$ of V_B^- spins is[32]

$$\Gamma_{1,Gd} \approx \frac{21\cdot 10^3 \pi N_A C_{Gd}}{8d^3} \frac{(\pi\mu_0\hbar\gamma_e\gamma_{Gd})^2\omega_{Gd}}{\omega_{Gd}^2 + 4\pi^2 D_{gs}^2} \quad (1)$$

where C_{Gd} is the Gd^{3+} concentration in mol·l^{-1}, N_A is the Avogadro number, μ_0 is the vacuum permeability, d is the average mean depth of the V_B^- defects, and $\gamma_{Gd} \approx \gamma_e \approx$ 28.0 GHz/T is the gyromagnetic ratio of electrons. $\omega_{Gd} \approx 50 \times 10^9$ s^{-1} + C_{Gd} · (77 × 10^9 s^{-1} M^{-1}).[32] Invoking this relaxation

https://doi.org/10.1021/acsphotonics.3c00621
ACS Photonics 2023, 10, 2894−2900

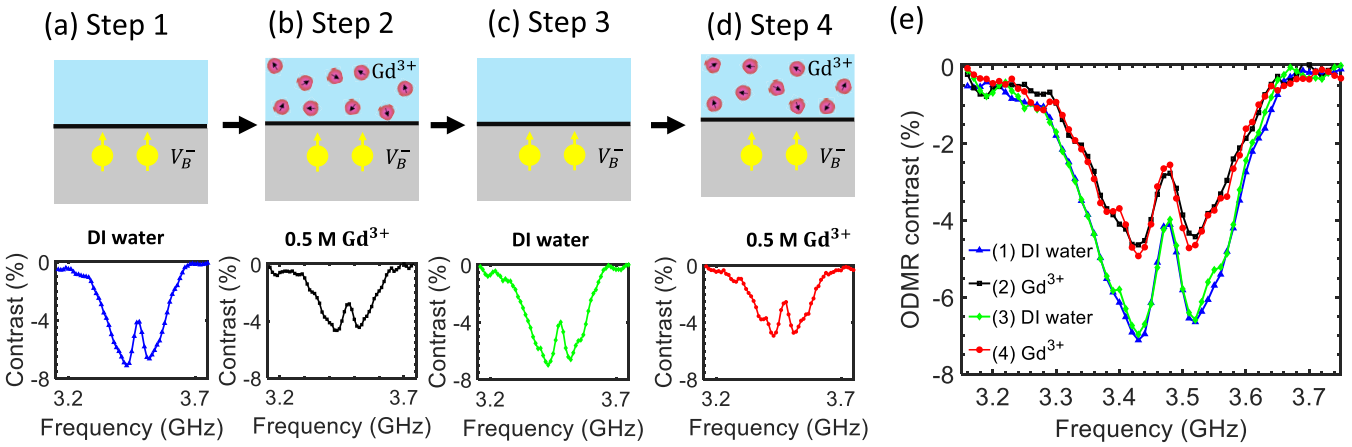

Figure 3. Reproducibility of the reduction of the ODMR contrast of shallow hBN spin defects due to liquid paramagnetic ions. Top panels: Illustration of CW ODMR experiments in DI water (a), 0.5 M Gd^{3+} solution (b), DI water (c), and 0.5 M Gd^{3+} solution (d). Steps 1−4 are performed in sequence. Bottom panels: CW ODMR results of Steps 1−4. Step 2 and Step 4 show the same amount of reduction in ODMR contrasts due to 0.5 M Gd^{3+} solutions. (e) Summary of the ODMR spectra in (a)−(d) for comparison. No external magnetic field is applied. The average depth of spin defects is 6.4 nm (Sensor 1).

model, the theoretical prediction shows good agreement with the experimental results for both sensors with different depths as shown in Figure 2f. This agreement further confirms that we have observed paramagnetic spin noise in liquids with hBN spin defects.

For the spin relaxometry measurements, the signal-to-noise ratio (SNR) of measuring the Gd^{3+} induced spin relaxation rate $\Gamma_{1,Gd}$ can be estimated by[48]

$$\mathrm{SNR} \approx \frac{\Gamma_{1,\mathrm{Gd}}}{\sqrt{\Gamma_1}} C \sqrt{\frac{\mathcal{R} T_{\mathrm{int}} \Delta t}{2e}} \tag{2}$$

where Γ_1 is the intrinsic relaxation rate of the spin defects, C is the contrast, $\mathcal{R}$ is the photon count rate under CW optical illumination, T_{int} is the width of the integration time window for each pulsed measurement, and Δt is the total acquisition time. With a typical photon count rate of 2×10^5 counts/s, a contrast of $C \sim 0.1$, an integration time of $T_{\mathrm{int}} = 200$ ns, and an intrinsic relaxation rate of $1/(14\ \mu s)$, the smallest Gd^{3+}-induced relaxation rate $\Gamma_{1,Gd}$ that can be detected with an SNR of 1 is around 31 $(\mathrm{ms})^{-1}/\sqrt{\mathrm{Hz}}$. Based on Figure 2f, this corresponds to a Gd^{3+} concentration sensitivity of about 0.5 $\mathrm{M}/\sqrt{\mathrm{Hz}}$ for Sensor 2 ($d = 4.5$ nm). Due to the small sensing volume ($\sim 10^{-21}$ m^3), the corresponding detection sensitivity of the amount of Gd^{3+} ions is about 10^{-18} $\mathrm{mol}/\sqrt{\mathrm{Hz}}$.

After demonstrating the capability of spin relaxometry, we develop another detection method based on the reduction of the ODMR contrast of hBN spin defects due to paramagnetic ions. In the pulsed spin relaxometry measurements, we observe a decrease in the contrast of V_B^- spin relaxation signal in the presence of Gd^{3+} ions (Figure 2d). Similar phenomena can also be observed in CW ODMR experiments. In DI water, V_B^- defects (Sensor 1, $d = 6.4$ nm) exhibit ~7% ODMR contrast under a 50 mW microwave driving (Figure 3a). Once the 0.5 M Gd^{3+} water solution replaces the DI water, we observe a dramatic reduction of ODMR contrast to less than 5% (Figure 3b). The ODMR contrast will resume after pumping the DI water back into the microfluid cell (Figure 3c) and will decrease again in the presence of Gd^{3+} solution (Figure 3d). Thus, the reduction of ODMR contrast due to paramagnetic ions is reversible and repeatable (Figure 3e). This method allows us to detect paramagnetic ions by monitoring the change in CW ODMR contrasts.

To quantify the dependence of the ODMR contrast on paramagnetic ion concentration, we perform the CW ODMR experiments in Gd^{3+} solutions with different concentrations from 0 to 1 M. As the concentration of Gd^{3+} increases, we observe a continuous reduction in the ODMR contrast (Figure 4). To quantify this concentration dependency, we select data points within the frequency range of 3.40−3.45 GHz and calculate the average ODMR contrasts (Figure 4b,d). The effect of Gd^{3+} ions at a concentration as low as 10 mM is observable. This method requires only a few ODMR data points to calculate the average integrated ODMR contrast and

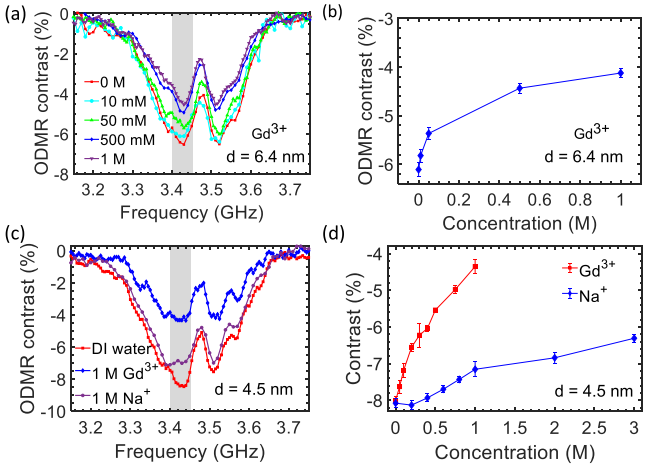

Figure 4. Effects of Gd^{3+} concentration on the V_B^- ODMR contrast. (a) ODMR spectra for several different Gd^{3+}-ion concentrations taken with Sensor 1 ($d = 6.4$ nm). All measurements are performed under a 50 mW microwave drive. (b) Averaged ODMR contrast in the 3.40 GHz to 3.45 GHz frequency range (gray box in (a)) as a function of Gd^{3+}-ion concentration. (c) ODMR spectra of Sensor 2 ($d = 4.5$ nm) in DI water (red squares), 1 M Na^+ solution (violet circles), and 1 M Gd^{3+} solution (blue diamonds). (d) Averaged ODMR contrast in the 3.40−3.45 GHz frequency range (gray box in (c)) as a function of Gd^{3+}- or Na^+-ion concentration. Gd^{3+} ions have a much larger effect on the ODMR contrast than Na^+ ions.

https://doi.org/10.1021/acsphotonics.3c00621
ACS Photonics 2023, 10, 2894−2900

does not rely on pulsed laser excitation, precise microwave manipulation, fast photodetectors, or multichannel pulse generators. This simplicity allows for rapid detection of paramagnetic ions in liquids, making it ideal for real-world applications.

The reduction of the ODMR contrast can be explained by the Gd^{3+} induced depopulation of the $m_s = 0$ ground state during the laser initialization, which has also been observed with diamond NV centers.[37,38] While a green laser tries to initialize spin defects to the $m_s = 0$ state, high-frequency magnetic noise will drive spin transitions from the $m_s = 0$ state to the $m_s = \pm 1$ states. In a solution of paramagnetic ions, a higher spin concentration gives rise to more magnetic noise due to spin fluctuations. A stronger spin relaxation effect due to spin noise will result in a lower spin polarization level for a given laser power, which gives rise to the concentration-dependent ODMR contrast reduction in shallow hBN spin defects. Additionally, Gd^{3+} ions can affect solution conductivity and cause slight microwave absorption, which can also impact the ODMR contrast of hBN spin defects. To identify the source of the ODMR contrast reduction, we compare the effects of Gd^{3+} ions and Na^+ ions on Sensor 2 (d = 4.5 nm). Na^+ ions are prepared by dissolving NaCl in water. Both the Na^+ and Cl^- ions are nonparamagnetic ions that will not generate spin noise at the location of V_B^- spin defects, and thus the reduction of the ODMR contrast in a NaCl solution comes from the microwave absorption by the solution. The observed reduction of ODMR contrast due to a NaCl solution is much smaller than that due to Gd^{3+} ions (Figure 4c,d). This indicates that the spin noise of Gd^{3+} ions is the major source of Gd^{3+}-induced ODMR contrast reduction. In the future, to mitigate the effect of microwave absorption, we can reduce the width of the microfluid channel to expose only a small portion of the microwave waveguide to the ionic solution. Furthermore, we can employ two hBN nanosheets with spin defects at two different depths: shallow spin defects can detect the spin noise of paramagnetic ions, while deep spin defects can monitor any potential ODMR contrast reduction due to microwave absorption by the ionic solution. Overall, the concentration-sensitive ODMR contrast allows for efficient detection of paramagnetic ions in liquids using CW ODMR, which is much simpler to implement than pulsed sensing protocols.

CONCLUSIONS

In conclusion, we have demonstrated the first detection of spin noise from paramagnetic ions in liquids using a vdW sensor based on hBN spin defects. Our spin relaxometry measurements reveal the characteristic behavior of the Gd^{3+}-induced spin relaxation, which increases with increasing Gd^{3+} concentration. By using the CW ODMR technique, we are also able to detect the Gd^{3+} ions via the contrast reduction of the spin-dependent PL. Our work represents an initial demonstration of the potential of hBN spin defects for paramagnetic ion sensing in liquids. There are many ways for further improvement. For instance, the sensitivity can be further improved by optimizing the hBN sensor, including reducing the depth of spin defects and improving the collection efficiency of the spin-dependent fluorescence. Future studies can also explore the sensing performance of hBN spin defects in more complex chemical and biological environments.

AUTHOR INFORMATION

Corresponding Author

Tongcang Li − *Department of Physics and Astronomy, Purdue University, West Lafayette, Indiana 47907, United States; Elmore Family School of Electrical and Computer Engineering, Birck Nanotechnology Center, and Purdue Quantum Science and Engineering Institute, Purdue University, West Lafayette, Indiana 47907, United States;* orcid.org/0000-0003-3308-8718; Email: tcli@purdue.edu

Authors

Xingyu Gao − *Department of Physics and Astronomy, Purdue University, West Lafayette, Indiana 47907, United States*

Sumukh Vaidya − *Department of Physics and Astronomy, Purdue University, West Lafayette, Indiana 47907, United States;* orcid.org/0000-0002-9732-6829

Peng Ju − *Department of Physics and Astronomy, Purdue University, West Lafayette, Indiana 47907, United States;* orcid.org/0000-0002-1128-7858

Saakshi Dikshit − *Elmore Family School of Electrical and Computer Engineering, Purdue University, West Lafayette, Indiana 47907, United States*

Kunhong Shen − *Department of Physics and Astronomy, Purdue University, West Lafayette, Indiana 47907, United States*

Yong P. Chen − *Department of Physics and Astronomy, Purdue University, West Lafayette, Indiana 47907, United States; Elmore Family School of Electrical and Computer Engineering, Birck Nanotechnology Center, and Purdue Quantum Science and Engineering Institute, Purdue University, West Lafayette, Indiana 47907, United States*

Complete contact information is available at: https://pubs.acs.org/10.1021/acsphotonics.3c00621

Funding

DARPA ARRIVE program; Quantum Science Center, a U.S. Department of Energy, Office of Science, National Quantum Information Science Research Center.

Notes

The authors declare no competing financial interest.

While finalizing this paper, we became aware of a related paper on detecting paramagnetic ions with hBN spin defects.[49]

REFERENCES

(1) Degen, C. L.; Reinhard, F.; Cappellaro, P. Quantum sensing. *Rev. Mod. Phys.* **2017**, *89*, No. 035002.

(2) Budker, D.; Romalis, M. Optical magnetometry. *Nat. Phys.* **2007**, *3*, 227−234.

(3) Schirhagl, R.; Chang, K.; Loretz, M.; Degen, C. L. Nitrogen-vacancy centers in diamond: nanoscale sensors for physics and biology. *Annu. Rev. Phys. Chem* **2014**, *65*, 83−105.

(4) Kucsko, G.; Maurer, P. C.; Yao, N. Y.; Kubo, M.; Noh, H. J.; Lo, P. K.; Park, H.; Lukin, M. D. Nanometre-scale thermometry in a living cell. *Nature* **2013**, *500*, 54−58.

(5) Casola, F.; Van Der Sar, T.; Yacoby, A. Probing condensed matter physics with magnetometry based on nitrogen-vacancy centres in diamond. *Nat. Rev. Mater.* **2018**, *3*, No. 17088.

(6) Shi, F.; Kong, F.; Zhao, P.; Zhang, X.; Chen, M.; Chen, S.; Zhang, Q.; Wang, M.; Ye, X.; Wang, Z.; et al. Single-DNA electron spin resonance spectroscopy in aqueous solutions. *Nat. Methods* **2018**, *15*, 697−699.

(7) Gottscholl, A.; Kianinia, M.; Soltamov, V.; Orlinskii, S.; Mamin, G.; Bradac, C.; Kasper, C.; Krambrock, K.; Sperlich, A.; Toth, M.;

et al. Initialization and read-out of intrinsic spin defects in a van der Waals crystal at room temperature. *Nat. Mater.* **2020**, *19*, 540−545.
(8) Gottscholl, A.; Diez, M.; Soltamov, V.; Kasper, C.; Sperlich, A.; Kianinia, M.; Bradac, C.; Aharonovich, I.; Dyakonov, V. Room temperature coherent control of spin defects in hexagonal boron nitride. *Sci. Adv.* **2021**, *7*, No. eabf3630.
(9) Mendelson, N.; Chugh, D.; Reimers, J. R.; Cheng, T. S.; Gottscholl, A.; Long, H.; Mellor, C. J.; Zettl, A.; Dyakonov, V.; Beton, P. H.; et al. Identifying carbon as the source of visible single-photon emission from hexagonal boron nitride. *Nat. Mater.* **2021**, *20*, 321−328.
(10) Chejanovsky, N.; Mukherjee, A.; Geng, J.; Chen, Y.-C.; Kim, Y.; Denisenko, A.; Finkler, A.; Taniguchi, T.; Watanabe, K.; Dasari, D. B. R.; et al. Single-spin resonance in a van der Waals embedded paramagnetic defect. *Nat. Mater.* **2021**, *20*, 1079−1084.
(11) Vaidya, S.; Gao, X.; Dikshit, S.; Aharonovich, I.; Li, T. Quantum sensing and imaging with spin defects in hexagonal boron nitride. *Adv. Phys.: X* **2023**, *8*, No. 2206049.
(12) Gao, X.; Jiang, B.; Llacsahuanga Allcca, A. E.; Shen, K.; Sadi, M. A.; Solanki, A. B.; Ju, P.; Xu, Z.; Upadhyaya, P.; Chen, Y. P.; et al. High-contrast plasmonic-enhanced shallow spin defects in hexagonal boron nitride for quantum sensing. *Nano Lett.* **2021**, *21*, 7708−7714.
(13) Novoselov, K. S.; Mishchenko, A.; Carvalho, A.; Castro Neto, A. H. 2D materials and van der Waals heterostructures. *Science* **2016**, *353*, No. aac9439.
(14) Huang, M.; Zhou, J.; Chen, D.; Lu, H.; McLaughlin, N. J.; Li, S.; Alghamdi, M.; Djugba, D.; Shi, J.; Wang, H.; Du, C. R. Wide field imaging of van der Waals ferromagnet Fe_3GeTe_2 by spin defects in hexagonal boron nitride. *Nat. Commun.* **2022**, *13*, No. 5369.
(15) Healey, A. J.; Scholten, S.; Yang, T.; Scott, J.; Abrahams, G.; Robertson, I.; Hou, X.; Guo, Y.; Rahman, S.; Lu, Y.; et al. Quantum microscopy with van der Waals heterostructures. *Nat. Phys.* **2023**, *19*, 87−91.
(16) Haykal, A.; Tanos, R.; Minotto, N.; Durand, A.; Fabre, F.; Li, J.; Edgar, J.; Ivady, V.; Gali, A.; Michel, T.; et al. Decoherence of V_B^- spin defects in monoisotopic hexagonal boron nitride. *Nat. Commun.* **2022**, *13*, No. 4347.
(17) Gottscholl, A.; Diez, M.; Soltamov, V.; Kasper, C.; Krauße, D.; Sperlich, A.; Kianinia, M.; Bradac, C.; Aharonovich, I.; Dyakonov, V. Spin defects in hBN as promising temperature, pressure and magnetic field quantum sensors. *Nat. Commun.* **2021**, *12*, No. 4480.
(18) Liu, W.; Li, Z.-P.; Yang, Y.-Z.; Yu, S.; Meng, Y.; Wang, Z.-A.; Li, Z.-C.; Guo, N.-J.; Yan, F.-F.; Li, Q.; et al. Temperature-dependent energy-level shifts of spin defects in hexagonal boron nitride. *ACS Photonics* **2021**, *8*, 1889−1895.
(19) Yang, T.; Mendelson, N.; Li, C.; Gottscholl, A.; Scott, J.; Kianinia, M.; Dyakonov, V.; Toth, M.; Aharonovich, I. Spin defects in hexagonal boron nitride for strain sensing on nanopillar arrays. *Nanoscale* **2022**, *14*, 5239−5244.
(20) Lyu, X.; Tan, Q.; Wu, L.; Zhang, C.; Zhang, Z.; Mu, Z.; Zúñiga-Pérez, J.; Cai, H.; Gao, W. Strain Quantum Sensing with Spin Defects in Hexagonal Boron Nitride. *Nano Lett.* **2022**, *22*, 6553−6559.
(21) Gao, X.; Vaidya, S.; Li, K.; Ju, P.; Jiang, B.; Xu, Z.; Allcca, A. E. L.; Shen, K.; Taniguchi, T.; Watanabe, K.; et al. Nuclear spin polarization and control in hexagonal boron nitride. *Nat. Mater.* **2022**, *21*, 1024−1028.
(22) Glushkov, E.; Macha, M.; Räth, E.; Navikas, V.; Ronceray, N.; Cheon, C. Y.; Ahmed, A.; Avsar, A.; Watanabe, K.; Taniguchi, T.; et al. Engineering optically active defects in hexagonal boron nitride using focused ion beam and water. *ACS Nano* **2022**, *16*, 3695−3703.
(23) Thomas, D. D. Breathing new life into nitric oxide signaling: a brief overview of the interplay between oxygen and nitric oxide. *Redox biology* **2015**, *5*, 225−233.
(24) Bogdan, C. Nitric oxide synthase in innate and adaptive immunity: an update. *Trends in immunology* **2015**, *36*, 161−178.
(25) Griendling, K. K.; Touyz, R. M.; Zweier, J. L.; Dikalov, S.; Chilian, W.; Chen, Y.-R.; Harrison, D. G.; Bhatnagar, A. Measurement of reactive oxygen species, reactive nitrogen species, and redox-dependent signaling in the cardiovascular system: a scientific statement from the American Heart Association. *Circ. Res.* **2016**, *119*, e39−e75.
(26) Weinmann, H.-J.; Brasch, R. C.; Press, W.-R.; Wesbey, G. E. Characteristics of gadolinium-DTPA complex: a potential NMR contrast agent. *Am. J. Roentgenol.* **1984**, *142*, 619−624.
(27) Chan, K. W.-Y.; Wong, W.-T. Small molecular gadolinium (III) complexes as MRI contrast agents for diagnostic imaging. *Coord. Chem. Rev.* **2007**, *251*, 2428−2451.
(28) Tweedle, M. F. Gadolinium Retention in Human Brain, Bone, and Skin. *Radiology* **2021**, *300*, 570−571.
(29) Pinheiro dos Santos, T. J.; Parambathu, A. V.; Fraenza, C. C.; Walsh, C.; Greenbaum, S. G.; Chapman, W. G.; Asthagiri, D.; Singer, P. M. Thermal and concentration effects on ^1H NMR relaxation of Gd^{3+}-aqua using MD simulations and measurements. *Phys. Chem. Chem. Phys.* **2022**, *24*, 27964−27975.
(30) Ma, L.; Azad, M. G.; Dharmasivam, M.; Richardson, V.; Quinn, R.; Feng, Y.; Pountney, D.; Tonissen, K.; Mellick, G.; Yanatori, I.; et al. Parkinson's disease: alterations in iron and redox biology as a key to unlock therapeutic strategies. *Redox Biol.* **2021**, *41*, No. 101896.
(31) Samrot, A. V.; Sahithya, C. S.; Selvarani, J.; Purayil, S. K.; Ponnaiah, P. A review on synthesis, characterization and potential biological applications of superparamagnetic iron oxide nanoparticles. *Curr. Res. Green Sustainable Chem.* **2021**, *4*, No. 100042.
(32) Steinert, S.; Ziem, F.; Hall, L.; Zappe, A.; Schweikert, M.; Götz, N.; Aird, A.; Balasubramanian, G.; Hollenberg, L.; Wrachtrup, J. Magnetic spin imaging under ambient conditions with sub-cellular resolution. *Nat. Commun.* **2013**, *4*, No. 1607.
(33) Ziem, F. C.; Gotz, N. S.; Zappe, A.; Steinert, S.; Wrachtrup, J. Highly sensitive detection of physiological spins in a microfluidic device. *Nano Lett.* **2013**, *13*, 4093−4098.
(34) Ermakova, A.; Pramanik, G.; Cai, J.-M.; Algara-Siller, G.; Kaiser, U.; Weil, T.; Tzeng, Y.-K.; Chang, H.-C.; McGuinness, L.; Plenio, M. B.; et al. Detection of a few metallo-protein molecules using color centers in nanodiamonds. *Nano Lett.* **2013**, *13*, 3305−3309.
(35) Shi, F.; Zhang, Q.; Wang, P.; Sun, H.; Wang, J.; Rong, X.; Chen, M.; Ju, C.; Reinhard, F.; Chen, H.; et al. Single-protein spin resonance spectroscopy under ambient conditions. *Science* **2015**, *347*, 1135−1138.
(36) Simpson, D. A.; Ryan, R. G.; Hall, L. T.; Panchenko, E.; Drew, S. C.; Petrou, S.; Donnelly, P. S.; Mulvaney, P.; Hollenberg, L. C. Electron paramagnetic resonance microscopy using spins in diamond under ambient conditions. *Nat. Commun.* **2017**, *8*, No. 458.
(37) Gorrini, F.; Giri, R.; Avalos, C.; Tambalo, S.; Mannucci, S.; Basso, L.; Bazzanella, N.; Dorigoni, C.; Cazzanelli, M.; Marzola, P.; et al. Fast and sensitive detection of paramagnetic species using coupled charge and spin dynamics in strongly fluorescent nanodiamonds. *ACS Appl. Mater. Interfaces* **2019**, *11*, 24412−24422.
(38) Radu, V.; Price, J. C.; Levett, S. J.; Narayanasamy, K. K.; Bateman-Price, T. D.; Wilson, P. B.; Mather, M. L. Dynamic quantum sensing of paramagnetic species using nitrogen-vacancy centers in diamond. *ACS Sens.* **2020**, *5*, 703−710.
(39) Liu, W.; Guo, N.-J.; Yu, S.; Meng, Y.; Li, Z.; Yang, Y.-Z.; Wang, Z.-A.; Zeng, X.-D.; Xie, L.-K.; Wang, J.-F.; et al. Spin-active defects in hexagonal boron nitride. *Mater. Quantum Technol.* **2022**, *2*, No. 032002.
(40) Xu, X.; Solanki, A. B.; Sychev, D.; Gao, X.; Peana, S.; Baburin, A. S.; Pagadala, K.; Martin, Z. O.; Chowdhury, S. N.; Chen, Y. P.; et al. Greatly Enhanced Emission from Spin Defects in Hexagonal Boron Nitride Enabled by a Low-Loss Plasmonic Nanocavity. *Nano Lett.* **2023**, *23*, 25−33.
(41) Ivády, V.; Barcza, G.; Thiering, G.; Li, S.; Hamdi, H.; Chou, J.-P.; Legeza, Ö.; Gali, A. Ab initio theory of the negatively charged boron vacancy qubit in hexagonal boron nitride. *npj Comput. Mater.* **2020**, *6*, No. 41.
(42) Mathur, N.; Mukherjee, A.; Gao, X.; Luo, J.; McCullian, B. A.; Li, T.; Vamivakas, A. N.; Fuchs, G. D. Excited-state spin-resonance spectroscopy of V_B^- defect centers in hexagonal boron nitride. *Nat. Commun.* **2022**, *13*, No. 3233.

https://doi.org/10.1021/acsphotonics.3c00621
ACS Photonics 2023, 10, 2894−2900

(43) Baber, S.; Malein, R. N. E.; Khatri, P.; Keatley, P. S.; Guo, S.; Withers, F.; Ramsay, A. J.; Luxmoore, I. J. Excited state spectroscopy of boron vacancy defects in hexagonal boron nitride using time-resolved optically detected magnetic resonance. *Nano Lett.* **2022**, *22*, 461−467.
(44) Mu, Z.; Cai, H.; Chen, D.; Kenny, J.; Jiang, Z.; Ru, S.; Lyu, X.; Koh, T. S.; Liu, X.; Aharonovich, I.; Gao, W. Excited-state optically detected magnetic resonance of spin defects in hexagonal boron nitride. *Phys. Rev. Lett.* **2022**, *128*, No. 216402.
(45) Yu, P.; Sun, H.; Wang, M.; Zhang, T.; Ye, X.; Zhou, J.; Liu, H.; Wang, C.-J.; Shi, F.; Wang, Y.; Du, J. Excited-state spectroscopy of spin defects in hexagonal boron nitride. *Nano Lett.* **2022**, *22*, 3545−3549.
(46) Ziegler, J. F.; Ziegler, M. D.; Biersack, J. P. SRIM−The stopping and range of ions in matter (2010). *Nucl. Instrum. Methods Phys. Res., Sect. B* **2010**, *268*, 1818−1823.
(47) Gong, R.; He, G.; Gao, X.; Ju, P.; Liu, Z.; Ye, B.; Henriksen, E. A.; Li, T.; Zu, C. Coherent dynamics of strongly interacting electronic spin defects in hexagonal boron nitride. *Nat. Commun.* **2023**, *14*, No. 3299.
(48) Tetienne, J.-P.; Hingant, T.; Rondin, L.; Cavaillès, A.; Mayer, L.; Dantelle, G.; Gacoin, T.; Wrachtrup, J.; Roch, J.-F.; Jacques, V. Spin relaxometry of single nitrogen-vacancy defects in diamond nanocrystals for magnetic noise sensing. *Phys. Rev. B: Condens. Matter Mater. Phys.* **2013**, *87*, No. 235436.
(49) Robertson, I. O.; Scholten, S. C.; Singh, P. et al. *Detection of Paramagnetic Spins with an Ultrathin van der Waals Quantum Sensor*. 2023, arXiv: 2302.10560. arXiv.org e-Print archive. https://arxiv.org/abs/2302.10560.

https://doi.org/10.1021/acsphotonics.3c00621
ACS Photonics 2023, 10, 2894−2900